

Energy Dissipation and Air Entrainment in Stepped Storm Waterway: Experimental Study

H. Chanson¹ and L. Toombes²

Abstract: For the last three decades, research focused on steep stepped chutes. Few studies considered flat-slope stepped geometries such as stepped storm waterways or culverts. In this study, experiments were conducted in a large, flat stepped chute ($\theta=3.4^\circ$) based upon a Froude similitude. Three basic flow regimes were observed: nappe flow without hydraulic jump, transition flow, and skimming flow. Detailed air–water flow measurements were conducted. The results allow a complete characterization of the air concentration and bubble count rate distributions, as well as an accurate estimate of the rate of energy dissipation. The flow resistance, expressed in terms of a modified friction slope, was found to be about 2.5 times greater than in smooth-chute flow. A comparison between smooth- and stepped-invert flows shows that greater aeration and larger residence times take place in the latter geometry. The result confirms the air–water mass transfer potential of stepped cascades, even for flat slopes ($\theta<5^\circ$).

DOI: 10.1061/(ASCE)0733-9437(2002)128:5(305)

CE Database keywords: Waterways; Air-water interaction; Energy dissipation; Air entrainment; Water flow; Culverts.

Introduction

The oldest stepped storm waterway is probably a series of Minoan stepped culverts in Knossos, Crete. The stepped culverts were designed to carry floodwater safely down the slope of the Vlychia valley beneath a road viaduct leading to the Knossos palace; the bridge was at least 10 m high and 5.5 m wide (Evans 1928). Three stepped waterways were excavated although more possibly existed. The steps were made of “squared ashlar masonry” with hard clay mortar. It is believed that the viaduct and stepped culverts were built during the Minoan period (B.C. 1500).

Modern applications of stepped waterways include stepped road gutters, city storm water systems, and sewers (Fig. 1). Stepped cascades are utilized also in water treatment plants. Artificial stepped cascades and drop structures can be introduced along or beside rivers and streams to reoxygenate waters with low dissolved oxygen contents. Near Chicago, five artificial cascades were designed along a waterway system to help the reoxygenation of the polluted canal (Robison 1994). Aesthetical applications of stepped cascades include stepped cascades and fountains in parks (e.g., at Versailles and St. Petersburg) and in cities (e.g., in Brisbane, Hong Kong, Taipei, and Tokyo).

¹Reader, Fluid Mechanics, Hydraulics, and Environmental Engineering, Dept. of Civil Engineering, Univ. of Queensland, Brisbane QLD 4072, Australia. E-mail: h.chanson@mailbox.uq.edu.au

²Assistant Lecturer, Dept. of Civil Engineering, Univ. of Queensland, Brisbane QLD 4072, Australia.

Note. Discussion open until March 1, 2003. Separate discussions must be submitted for individual papers. To extend the closing date by one month, a written request must be filed with the ASCE Managing Editor. The manuscript for this paper was submitted for review and possible publication on June 28, 2001; approved on January 2, 2002. This paper is part of the *Journal of Irrigation and Drainage Engineering*, Vol. 128, No. 5, October 1, 2002. ©ASCE, ISSN 0733-9437/2002/5-305–315/\$8.00+\$0.50 per page.

Bibliographic Review

For a given (flat) stepped geometry, low flows behave as a series of free-falling nappe and nappe impact on the downstream step (i.e., nappe flow). For large flow rates, the water skims over the steps and it is called a skimming flow regime (e.g., Rajaratnam 1990; Chanson 1995a, 1996) and Ohtsu and Yasuda



Fig. 1. Stepped stormwater beneath the Univ. of Hong Kong

Table 1. Summary of Experimental Flow Conditions

Reference	Slope θ (deg)	h	l	q_w (m ² /s)	d_0 (m)	Comments
Present study (UQ) ^a						
Smooth chute	4.0	N/A ^b	N/A	0.142 to 0.164	0.03	$L=25$ m. $W=0.5$ m. Painted timber
Stepped chute						
Series 1a	3.4 ^c	0.143	2.4	0.04 to 0.150	0.03	$L=25$ m, $W=0.5$. Horizontal timber steps. (No sidewall offset at 1st drop)
Series 1b	3.4 ^c	0.143	2.4	0.080 to 0.150	0.03	$L=25$ m, $W=0.5$ m. Horizontal timber steps. Sidewall offset for nappe ventilation at 1st drop (only).
Series 2	3.4 ^a	0.071	1.2	0.080 to 0.150	0.03	$L=25$ m, $W=0.5$ m. Horizontal timber steps. Sidewall offset for nappe ventilation at 1st drop (only). First drop located 2.4 m downstream of intake.
Yasuda and Ohtsu (1999)						
Smooth chute	5.7	N/A	N/A	0.008 to 0.08	N/A	$L=7$ m, $W=0.4$ m. Uncontrolled ogee crest
Stepped chute						
	5.7	0.05	0.5	0.063 to 0.08	N/A	$L=7$ m, $W=0.4$ m. Uncontrolled ogee crest. Skimming flow conditions. Unventilated steps.
	5.7	0.025	0.25	0.022 to 0.08	N/A	$L=7$ m, $W=0.4$ m. Uncontrolled ogee crest. Skimming flow conditions. Unventilated steps.

Notes: d_0 =approach flow depth; h =step height; k_s =equivalent roughness height; L =channel length; l =step length; and q_w =water discharge per unit width.

^aUQ indicates the Univ. of Queensland.

^bN/A indicates not applicable.

^cLongitudinal slope of pseudobottom formed by step edges.

(1997) mentioned a transition flow pattern between the nappe and skimming flow for intermediary discharges.

For the last three decades, research focused on steep stepped chutes (Chanson 1995a). Few studies considered flat-slope stepped geometries. Noori (1984) studied skimming flows above 4 mm high steps with a 5.7° slope. The study was performed with low-velocity flows, and the results were affected by scale effects associated with flow aeration and the difficulty to accurately machine the small steps. Chanson and Toombes (1997) presented early results of nappe flows down a 24 m long 3.4° slope chute ($h=143$ mm). Yasuda and Ohtsu (1999) investigated skimming flows down a 7 m long chute with a 5.7° slope and a large step heights ($h=25$ and 50 mm).

In the present study, new experiments were performed in a large-size facility (24 m long, 3.4° slope). Based upon a Froude similitude, the large size of the facility ensures that the experimental results may be extrapolated to prototype with minimum scale effects for geometric scaling ratios less than 10:1 (Wood 1991; Chanson 1997a). The results provide new information on the basic flow patterns, air entrainment, and energy dissipation. It is the purpose of this paper to critically assess the basic flow patterns, to present new analysis and experimental results, to compare these with existing data, and to propose new compelling conclusions regarding flat stepped storm waterways.

Experimental Apparatus and Method

New experiments were performed in a 24 m long 0.5 m wide flume previously used by Chanson (1997b) to investigate the flow properties down a smooth-invert chute. The flume was made of planed wooden boards (equivalent surface roughness height: 1 mm). Two stepped invert configurations were used (Table 1, Fig. 2). Experiments Series 1 were conducted with ten 0.143 m high 2.4 m long horizontal steps while Experiments Series 2 were performed with 18 0.071 m high 1.2 m long flat steps. The first drop was located 2.4 m downstream of a smooth nozzle, and the channel invert, upstream of the vertical drop, was flat and horizontal for all experiments.

Water was supplied by a pump, with a variable-speed electronic controller (Taian™ T-verter K1-420-M3 adjustable frequency ac motor drive), enabling an accurate discharge adjustment in a closed-circuit system. The flow rates were measured with a Dall™ tube flowmeter, calibrated on site. The accuracy of the discharge measurement was approximately 2%. Clear-water flow depths and velocities were measured with a point gauge and a Prandtl–Pitot tube ($\varnothing=3.3$ mm) respectively. Air–water flow properties were measured using a single-tip conductivity probe ($\varnothing=0.35$ mm) developed at the Univ. of Queensland (Chanson 1995b). The probe was aligned in the flow direction and excited by an air bubble detector (AS25240). The resistivity probe signal was scanned at 5 kHz for 60 sec (Series 1) to 180 sec

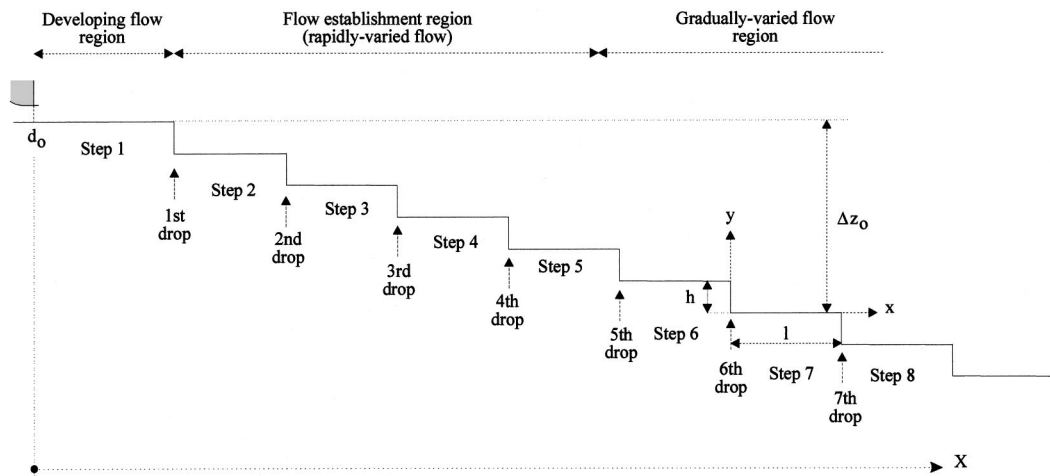


Fig. 2. Sketch of experimental facility

(Series 2). The translation of the probe in the direction normal to the channel invert was controlled by a fine adjustment traveling mechanism connected to a Mitutoyo™ digimatic scale unit (Ref. No. 572-503). The error on the vertical position of the probe was less than 0.025 mm. The system (probe and traveling mechanism) was mounted on a trolley system. The accuracy of the longitudinal position of the probe was estimated as $\Delta x < \pm 0.5$ cm. The

accuracy of the transverse position of the probe was less than 1 mm.

For each flow rate, air–water measurements were performed at several steps, and at several longitudinal positions x on each step. Most data were recorded on the centerline, although some profiles were measured next to the sidewalls in the sidewall standing waves. (Unless indicated the results are centerline data).

Table 2. Flow Regime and Experimental Observations at Downstream End of Chute (Present Study)

Reference	Flow rate q_w	Flow regime	End Chute Data ^a						Remarks
			C_{mean}	Y_{90}/d_c	$\Delta H/H$	H_{res}/d_c	S_f	f	
Smooth chute	0.150	Smooth invert	0.09	0.365	0.76	4.84	0.0419	0.0154	Smooth invert
Series 1a	0.02	NA2	—	—	—	—	—	—	$h=0.143$ m Upper limit of hydraulic jump
	0.038	NA3	—	—	—	—	—	—	
	0.080	NA3	—	—	—	—	—	—	
	0.130	NA3	—	—	—	—	—	—	
	0.150	NA3	—	—	—	—	—	—	
	0.163	NA3	—	—	—	—	—	—	
	0.130	NA3	0.19	0.501	0.81	3.41	0.1116	0.0596	Air–water flow measurements ^b
	0.150	NA3	0.18	0.478	0.80	3.62	0.150	0.080	^b
Series 1b	0.080	NA3	0.20	0.544	0.83	3.05	0.0655	0.0287	$h=0.143$ m Run CR1 ^b
	0.110	NA3	0.18	0.510	0.81	3.31	0.0297	0.0153	Run CR2 ^b
	0.150	NA3	0.20	0.501	0.81	3.53	0.1812	0.0956	Run CR2 ^b
Series 2	0.080	TRA	0.22	0.515	0.79	3.49	0.0726	0.038	$h=0.071$ m Run ES1 ^b
	0.110	SK1	0.24	0.547	0.79	3.51	0.0373	0.0199	Run ES2 ^b
	0.150	SK1	0.24	0.429	0.72	5.03	0.084	0.0375	Run ES3 ^b

Notes: Flow regime: NA2=nappe flow with hydraulic jumps; NA3=nappe flow without hydraulic jump; TRA=transition flow; and SK1=skimming flow. End chute data: calculated based upon air–water flow properties.

^aEnd chute flow conditions measured at downstream end of step 9 (Series 1) and 16 (Series 2).

^bDetailed air–water flow measurements.

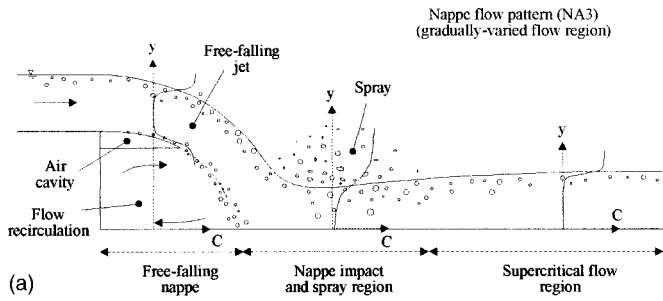


Fig. 3. Air entrainment in the nappe flow regime (Experiments Series 1): (a) sketch of basic flow pattern.

Inflow Conditions and Longitudinal Free-Surface Profiles

The flow to the 24 m long flume was fed through an elliptical nozzle (1.7 m long) and the nozzle exit was 30 mm high and 0.5 m wide. The measured contraction ratio was unity (i.e., $d_0 = 30$ mm). For all experiments, the inflow conditions were supercritical: $1.3 \leq F_0 \leq 10$ where F_0 is the approach flow Froude number.

At the upstream end (Step 1, Fig. 2), the supercritical flow was decelerated until it reached the first drop and little aeration was observed. Pitot tube measurements showed that the flow was two-dimensional and the boundary layer was fully developed immediately upstream of the first drop. Measured mean air concentrations of 7 to 12% (at $X = 2.4$ m) described the “wavy” nature (or roughness) of the free-surface rather than true self-aeration.

At the first brink (i.e., first vertical drop), the deflected nappe was a free-falling jet for all investigated flow conditions and the flow on Step 2 was highly turbulent (Chanson and Toombes 1997). For all the investigations (Series 1 and 2), the flow on

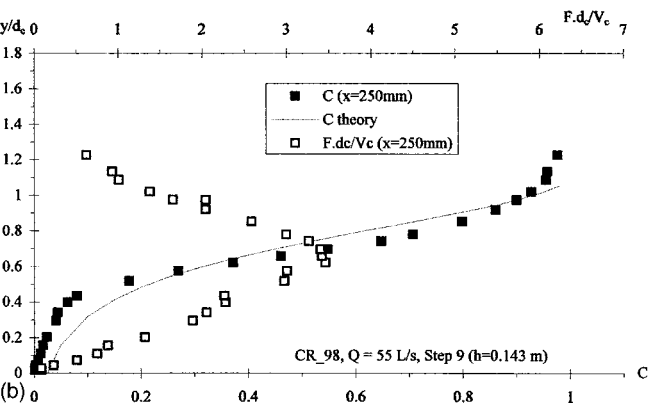
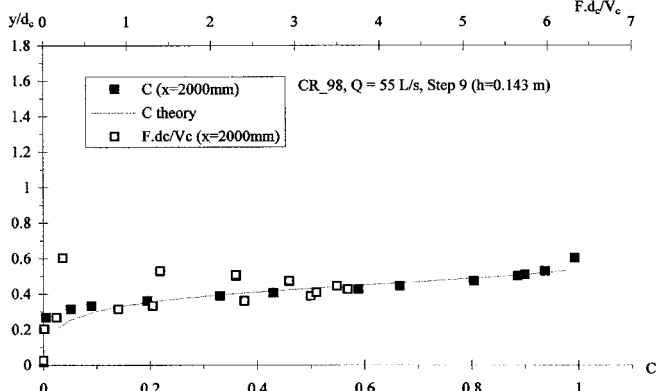
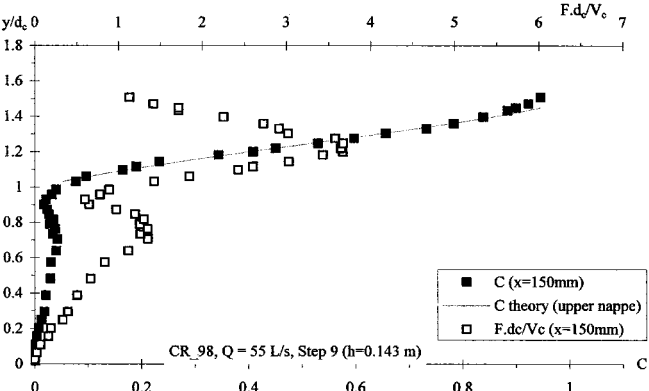
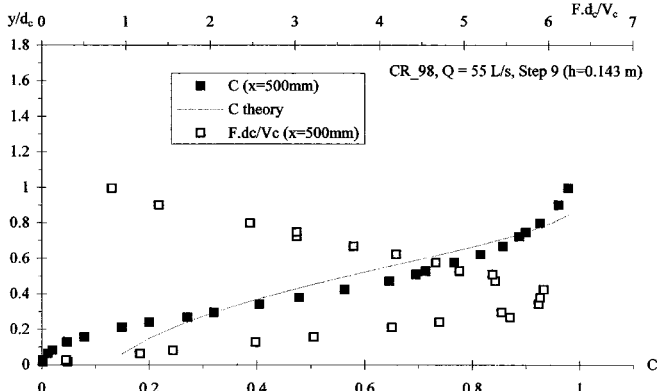
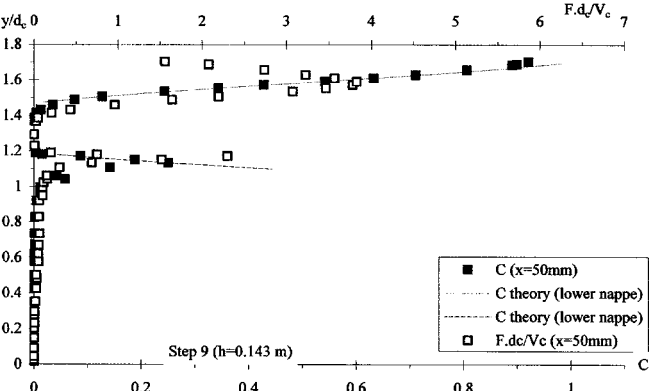


Fig. 3. Air entrainment in the nappe flow regime (Experiments Series 1): (b) dimensionless air concentration and bubble frequency distributions ($q_w = 0.11 \text{ m}^2/\text{s}$, $h = 0.143$ m, Step No. 9) at $x = 50, 150, 250, 500,$ and 2000 mm.

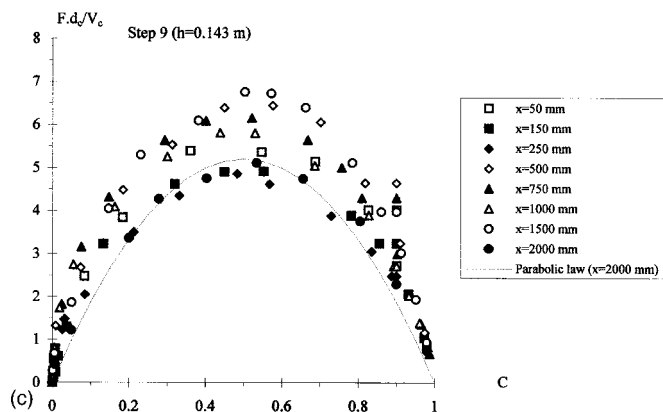


Fig. 3. Air entrainment in the nappe flow regime (Experiments Series 1): (c) dimensionless relationship between air concentration and air bubble frequency ($q_w=0.150 \text{ m}^2/\text{s}$, $h=0.143 \text{ m}$, Step No. 9).

Steps 2, 3, and 4 was rapidly varied and this region is a flow establishment zone characterized by three-dimensional flow patterns (e.g., shock waves and sidewall standing waves) and by significant changes in flow properties from one step to the next one. For example, shock waves were observed on Steps 2 and sometimes Step 4, but the cross waves were barely seen on Step 3. In addition, the rate of energy dissipation was significant at the first three drops: i.e., $\Delta H/H \approx 60$ to 65% in Series 1 and about 30 to 40% in Series 2. Further downstream (i.e., Step 5 onwards), the flow became gradually varied, with gradual variations of the flow properties from step to step.

Basic Flow Regimes

In the gradually varied flow region (i.e., downstream of flow establishment zone), the flow patterns were basically identical from one step to another, for a given flow rate and step height. The experimental flow conditions allowed investigations of nappe, transition, and skimming flow regimes (Table 2).

In experiments Series 1 ($h=0.143$), the flow was a succession of free-falling nappe, nappe impact, and supercritical flow on each step for all flow rates. That is, it was a nappe flow without hydraulic jump for $0.24 < d_c/h \leq 0.97$, where d_c is the critical depth and h is the step height.

In experiments Series 2, and for $d_c/h=1.2$, the flow pattern did not exhibit the quasismooth appearance of skimming flow, nor the succession of free-falling nappes as in nappe flow. Thus, it was a transition flow regime. At each step, the flow was characterized by a pool of recirculating waters, and significant spray and water deflection immediately downstream of the stagnation point. In the spray region, very high aeration was recorded with C_{mean} reaching up to 40%. Downstream, the supercritical flow was decelerated up to the downstream step edge and shock waves were observed.

In experiments Series 2, for $d_c/h > 1.2$, the flow was skimming over the step edges, (i.e., skimming flows) although a deflected nappe was observed at the first drop. The free surface was not parallel to the pseudobottom formed by the step edges but it exhibited an “undular” pattern in phase with the step geometry. A similar skimming flow pattern was observed by Yasuda and Ohtsu (1999) for $d_c/h \geq 1.45$ ($h=0.05 \text{ m}$).

Air–Water Flow Properties

Air Concentration Distributions

In nappe flow (Series 1), the upstream end of the step is characterized by a free-falling nappe, an air cavity, and a pool of recirculating fluid (Fig. 3). Air bubble entrainment occurs at both the upper and lower jet interfaces, with additional air being entrained by a plunging jet mechanism at the intersection of the lower nappe with the recirculating pool [Fig. 3(a)]. At the lower nappe, the developing shear layer is characterized by a high level of turbulence and significant interfacial air entrainment is observed. The latter may be modeled by an air diffusion model

$$C = \frac{1}{2} \left(1 - \operatorname{erf} \left(\frac{y - Y_{50}}{2 * \sqrt{\frac{D_t}{V} x}} \right) \right) \quad (1)$$

where C =the air concentration, y =the vertical coordinate, Y_{50} =the location where $C=50\%$, D_t =an average air bubble diffusivity, V =the jet velocity, x =the horizontal distance measured from the upstream step edge, and the function erf is defined as: $\operatorname{erf}(u) = 2/\sqrt{\pi} \int_0^u \exp(-t^2/2) dt$ (e.g., Chanson 1997a; Brattberg et al. 1998). At the upper nappe, the air entrainment process is more complex. The air–water interface is affected by turbulent eddies acting next to the free surface and by a rapid pressure redistribution downstream of the step brink. A modified solution of the diffusion equation was proposed for the upper nappe of spillway aeration devices:

$$C = \frac{1}{2} * \left(1 - \operatorname{erf} \left(\frac{Y_{50} - y}{2 \sqrt{\frac{D_t}{V} x \left(1 + k * \frac{Y_{50} - y}{x} \right)}} \right) \right) \quad (2)$$

where the quantity D_t and Y_{50} =those of the upper nappe, and k =a dimensionless parameter taking into account the pressure redistribution (Chanson 1989a). Eq. (2) however neglects the initial free-surface aeration, and it is not valid when the jet core becomes aerated. Eqs. (1) and (2) are compared with data in Fig. 3(b).

Immediately downstream of the nappe impact, a considerable spray was generated. Visual observations showed some large droplets reaching heights of up to 0.5 m above the invert. A strong flow aeration was recorded with the air concentration profiles: e.g., in Fig. 3(b) at $x=0.15$, 0.25 and 0.5 m. Further downstream, the supercritical flow was decelerated and the free-surface aeration was similar to that observed in self-aerated flows and in the flow downstream of an aeration device (e.g., Chanson 1989b). The distribution of air concentration may be described by a diffusion model

$$C = 1 - \tanh^2 \left(K' - \frac{y}{2 * D' Y_{90}} \right) \quad (3)$$

where \tanh =the hyperbolic tangent function, y =the distance normal to the invert, Y_{90} =the distance where $C=90\%$, D' =a dimensionless turbulent diffusivity, and K' =an integration constant (Chanson 1995b, 1997a). D' and K' are functions of the mean air content C_{mean} only and they may be estimated as

$$D' = \frac{0.848 C_{\text{mean}} - 0.00302}{1 + 1.1375 C_{\text{mean}} - 2.2925 C_{\text{mean}}^2} \quad C_{\text{mean}} < 0.7 \quad (4)$$

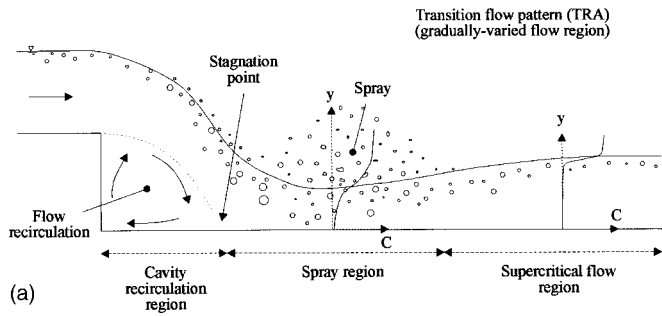


Fig. 4. Air entrainment in the transition flow regime (Experiments Series 2, $d_c/h=1.2$): (a) sketch of the flow patterns.

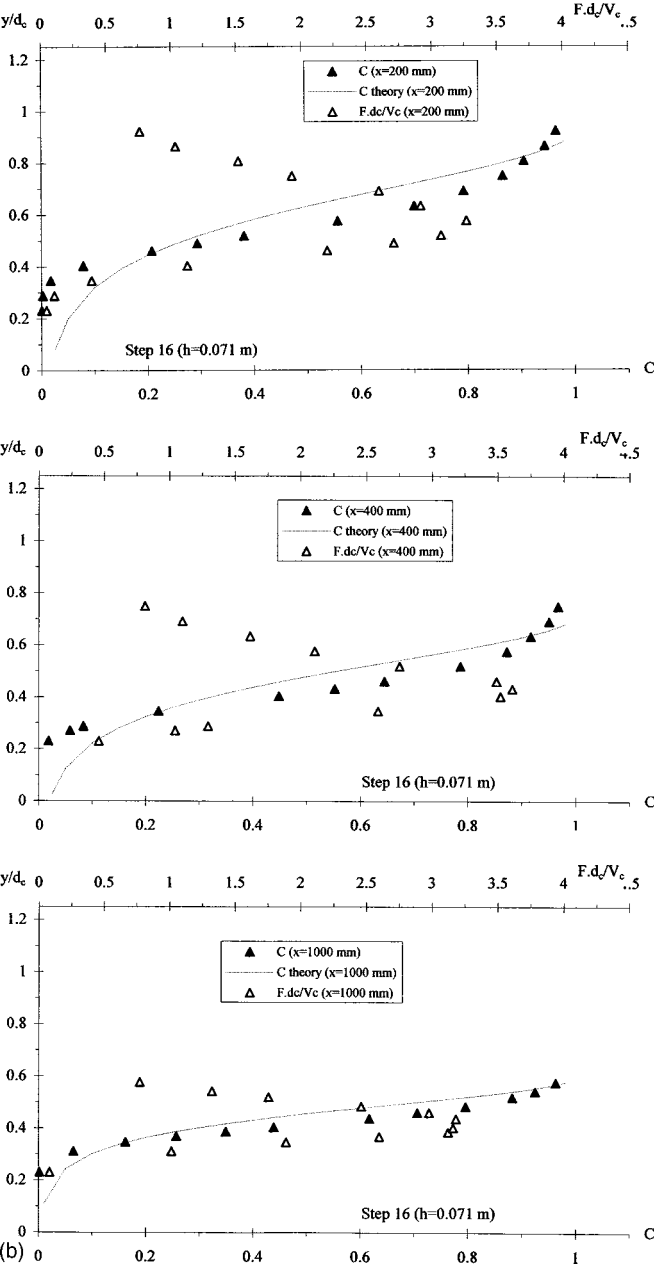


Fig. 4. Air entrainment in the transition flow regime (Experiments Series 2, $d_c/h=1.2$): (b) dimensionless air concentration and bubble frequency distributions ($q_w=0.08 \text{ m}^2/\text{s}$, $h=0.07 \text{ m}$, Step No. 16) at $x=200, 400, 1000 \text{ mm}$.

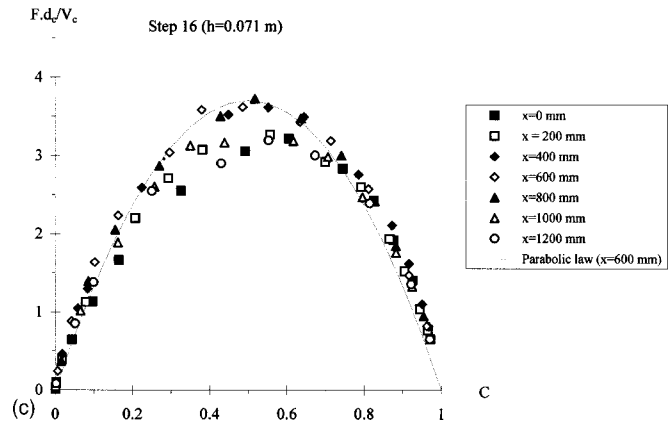


Fig. 4. Air entrainment in the transition flow regime (Experiments Series 2, $d_c/h=1.2$): (c) dimensionless relationship between air concentration and air bubble frequency ($q_w=0.08 \text{ m}^2/\text{s}$, $h=0.07 \text{ m}$, Step No. 16).

$$K' = 0.32745015 + \frac{0.5}{D'} \quad (5)$$

The mean air content C_{mean} is defined as: $(1 - C_{\text{mean}})Y_{90} = d$, where d is the clear-water depth: $d = \int_0^{Y_{90}} (1 - C) dy$. Eq. (3) was tested successfully in parts of the spray region and in the supercritical flow region (Fig. 3), although it was developed originally and validated for smooth-invert chute flow.

In the transition flow regime (Series 2, $d_c/h=1.2$), the flow pattern exhibited significant longitudinal variations along each step and it did not exhibit the quasismooth appearance observed in skimming flow. The transition flow was characterized by a pool of recirculating waters (i.e., absence of air cavity), and splashing and water deflection immediately downstream of the stagnation point [Fig. 4(a)]. A very significant spray region was observed and the (depth-averaged) mean air content was maximum. Further downstream, the supercritical flow was decelerated up to the downstream step edge. Eq. (3) compares favorably with the air concentration distributions in parts of both spray and supercritical flow regions [Fig. 4(b)].

In skimming flows (Series 2, $d_c/h > 1.2$), the flow at each step was characterized by longitudinal variations of the flow aeration. Maximum aeration was observed around $x/l \sim 0.3$ to 0.5 with gradual deaeration downstream, up to the next step brink. The air concentration distributions followed Eq. (3) [Fig. 5(a)].

Air Bubble Frequency Distributions

The bubble frequency or bubble count rate is defined as the number of bubbles impacting the robe tip per second. For a given flow velocity and void fraction, the bubble count rate F is inversely proportional to the mean bubble size, and directly proportional to the air–water specific interface area. Typical distributions are presented in Figs. 3, 4, and 5.

For all flow rates, the relationship between bubble frequency and air content was a quasiparabolic shape which is best fitted by

$$\frac{F}{F_{\text{max}}} = 1 - (1 - 2C)^2 \quad (6)$$

where the maximum bubble frequency F_{max} was observed for $C=50\%$ [Figs. 3(c), 4(c), and 5(b)]. The parabolic shape [i.e., Eq.

(6)] was observed first in open channel flows and later in high-velocity water jets and hydraulic jumps (Chanson 1997b; Brattberg et al. 1998; Chanson and Brattberg 2000). The result suggests a similarity of air–water flow patterns between the four flow situations.

In dimensionless terms, similar bubble count rates (Fd_c/V_c) were observed in nappe and skimming flows, while lower bubble frequencies were recorded in the transition flow, despite the greater splashing and spray observed in the latter (Fig. 4). The result implies that comparatively larger droplets and bubbles were detected in the transition flow.

Discussion

At the downstream end of the chute, the mean air content (measured at a step edge) ranged typically from 0.18 to 0.24 (Table 2, column 4) while greater depth-averaged air concentrations were measured between step edges. For comparison, the mean air content at the downstream end of the same chute equipped with a smooth invert was only 9% (Chanson 1997b).

Figure 6 presents further the longitudinal variations of the mean air content and dimensionless maximum bubble frequency along one step. Each graph includes one series of nappe, transition, and skimming flow data. In nappe flow, maximum aeration was consistently observed downstream of the plunge point [Fig. 6(a), gray circle, $x/l=0.3$ to 0.4], followed by downstream de-aeration. In transition and skimming flows, the longitudinal variations in C_{mean} were moderate although greater aeration was always observed in the middle of the step ($x/l\sim 0.3$ to 0.6) than at the step edges (e.g., $x/l=0$ and 1).

Longitudinal distributions of maximum dimensionless bubble frequency present some scatter [Fig. 6(b)]. Fig. 6(b), however, illustrates the lower bubble count rates observed in transition flows (Series 2, $q_w=0.08$ m²/s).

Energy Dissipation

Although many researchers present the rate of energy dissipation $\Delta H/H$, practicing engineers require information on the residual head to assess the need for a downstream stilling structure. Table 2, column 7 summarizes the dimensionless residual head H_{res}/d_c at the downstream end of the chute, where the total head H was calculated as

$$H = z_0 + d + \frac{U_w^2}{2g} \quad (7)$$

where U_w =flow velocity= q_w/d , q_w =the water discharge per unit width and d =the clear-water depth, and z_0 is the invert elevation. For all data, the clear water depth was measured in the supercritical flow immediately upstream of the step brink where the streamlines were parallel to the invert and the pressure distribution was hydrostatic. The smooth-invert data are also shown in Table 2. As a first estimate, the dimensionless residual head may be correlated as

$$\frac{H_{\text{res}}}{d_c} = 3.57 * \left(\frac{d_c}{h} \right)^{-0.36} \quad (8)$$

The rate of energy dissipation may also be expressed in terms of the friction slope $S_f = -\partial H / \partial z_0$, or a modified friction slope

$$\frac{S_f}{\frac{1}{8}F^2} \quad (9)$$

where F =local Froude number. For a wide channel, the energy equation (i.e., backwater equation) yields:

$$\frac{S_f}{\frac{1}{8}F^2} = \frac{\tau_0}{\frac{1}{8}\rho_w U_w^2} = f \quad (10)$$

where the right-hand side term is a dimensionless average boundary shear stress. On a smooth chute, the modified friction slope [Eq. (9)] is the Darcy–Weisbach friction factor f characterizing the friction loss. In nappe flow, it characterized the mean energy loss caused by jet disintegration, nappe impact, and friction loss downstream. The modified friction slope characterizes the form drag loss in skimming flow.

Kazemipour and Apelt (1983) stressed that to try to account for the form losses with a Darcy–Weisbach or even Gauckler–Manning formula is unsatisfactory. Nevertheless, it is still common practice, and this study is no exception. Experimental results are presented in Fig. 7 and Table 2 (column 9), showing the modified friction slope as a function of the relative step roughness ($h \cos \theta / D_H$), where θ is the slope of the pseudobottom formed by the step edges and D_H is the hydraulic diameter. Despite some scatter, which reflects in part the three different flow regimes (during the present study), the modified friction slope [Eq. (9)] of the stepped chute is in average about 2.5 times greater than the Darcy friction factor of the same smooth-invert chute. A similar result is observed with the data of Yasuda and Ohtsu (1999) ($h=0.05$ and 0.025 m).

Discussion

Table 2 presents a comparison of the air–water flow properties at the downstream end of the flume. It includes smooth-invert data and stepped chute data (recorded in the supercritical flow region near the downstream end of a step). First, the results highlight the greater flow depths associated with slower velocities observed in the stepped chutes. The data show also a greater aeration on the stepped cascades. This is illustrated in Fig. 8 showing air concentration distributions at the end of the chute for an identical flow rate and three invert geometries (smooth, $h=0.071$ m and $h=0.143$ m).

A detailed analysis of the bubble count rate distributions shows that the maximum dimensionless bubble count rate is of the same order of magnitude for both smooth and stepped geometries, but the depth-averaged bubble frequency is significantly greater on the stepped cascade. Together, the greater flow aeration and slower flow velocities in stepped chutes yield greater interfacial areas and residence time. Both effects combine to maximize gas transfer above a stepped cascade.

Analogy between Nappe Flow and Spillway Aeration Device Flows

There is some analogy between the nappe flow without hydraulic jump [Fig. 3(a)] and spillway aeration device flows (Fig. 9). Spillway aerators are designed to artificially introduce air into the high-velocity flow, to reduce or to prevent downstream cavitation damage. Detailed air–water flow studies of spillway aeration device models are summarized in Table 3.

Both types of flows are characterized by a free-falling nappe and nappe impact. Similar air entrainment processes are observed: i.e., interfacial aeration of the nappe, spray, and splashing at nappe impact and self-aeration downstream of the impact region. A main difference is possibly the strong interfacial aeration at aeration devices while aeration is maximum in the impact zone in nappe flows without hydraulic jump. The overall aeration perfor-

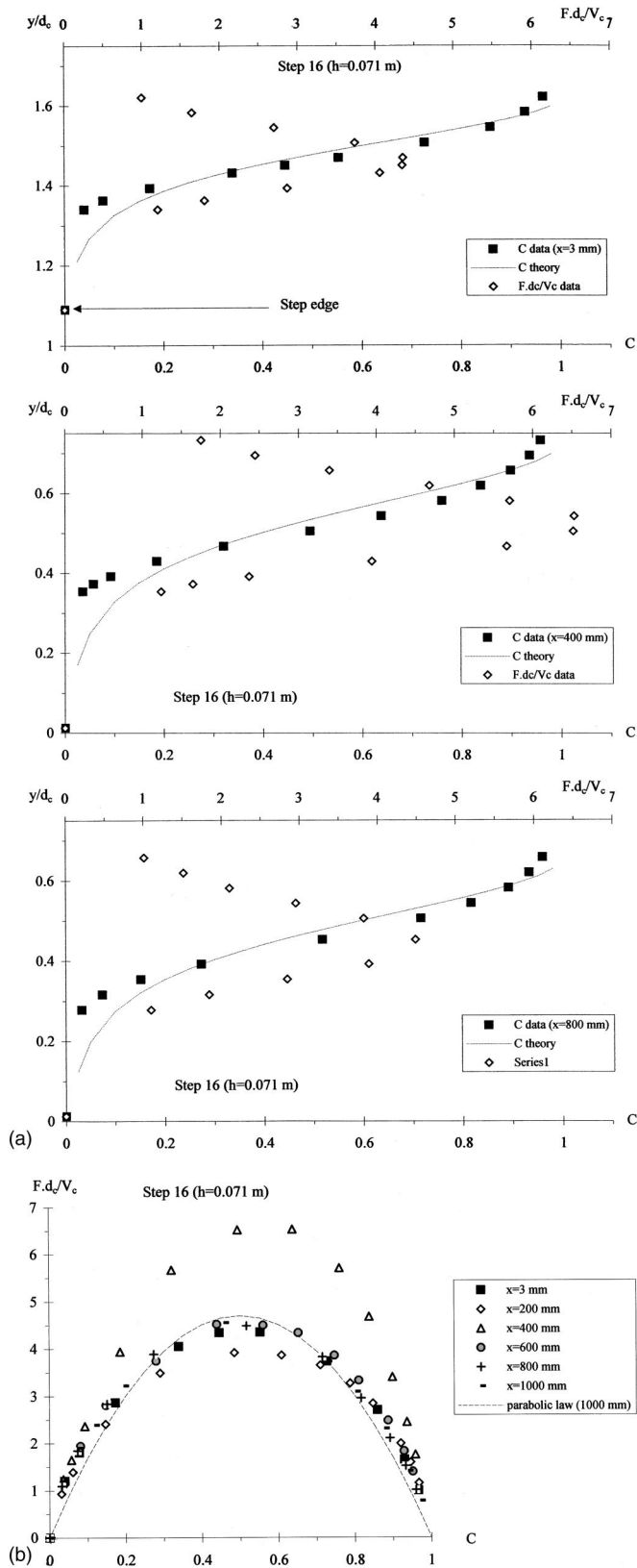


Fig. 5. Air entrainment in skimming flows (Experiments Series 2, $d_c/h > 1.2$): (a) dimensionless air concentration and bubble frequency distributions ($q_w = 0.15$ m²/s, $h = 0.07$ m, Step No. 16) at $x = 0, 400,$ and 800 mm and (b) dimensionless relationship between air concentration and air bubble frequency ($q_w = 0.15$ m²/s, $h = 0.07$ m, Step No. 16).

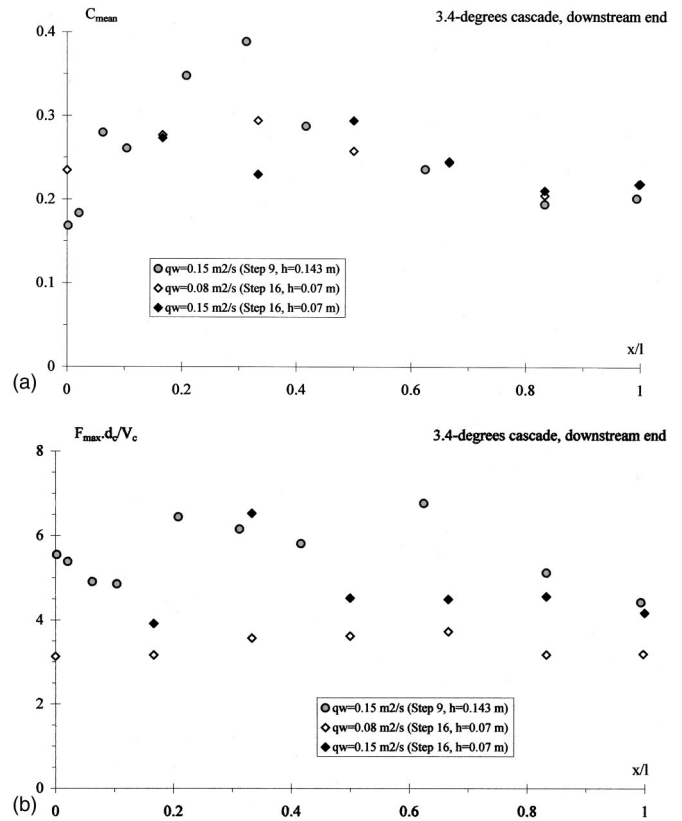


Fig. 6. Longitudinal variations of the mean air concentration and maximum air bubble frequency on a step (a) mean air concentrations and (b) dimensionless maximum bubble count rates $F_{max}d_c/V_c$.

mances of both nappe flow and spillway aerator is presented in Fig. 10, showing the mean air concentration at the downstream end of the impact region as a function of the inflow Froude number. The nappe flow data were measured at the first and eighth vertical drops (i.e., steps 2 and 9, respectively). Despite the scatter which reflects the wide range of geometries, Fig. 10 suggests that a nappe flow provides comparatively more aeration for a given Froude number than spillway aerators.

For the experimental data, the mean air content downstream of nappe impact may be roughly correlated by

$$C_{mean} = 0.21 + 0.018F \quad (11)$$

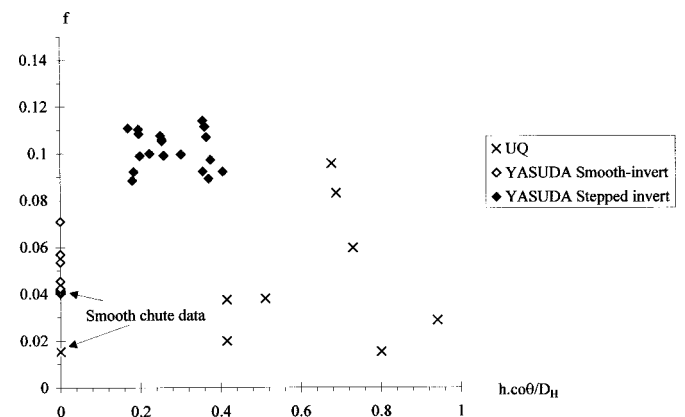


Fig. 7. Modified friction slope $8 S_f/F^2$ as function of dimensionless step roughness $h^* \cos \theta / D_H$

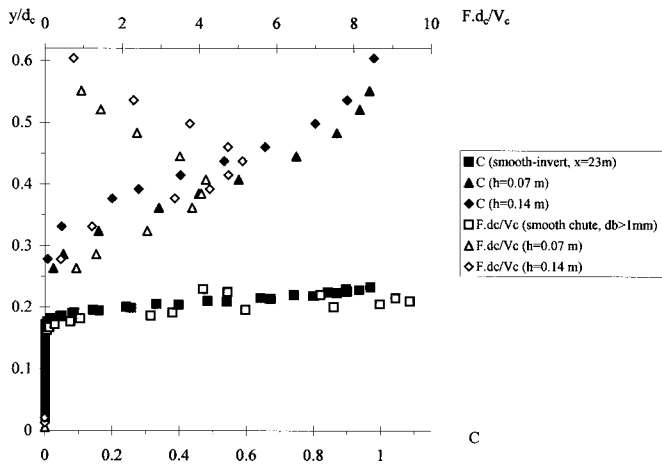


Fig. 8. Comparison between smooth-invert and stepped chute flows in the same flume for an identical flow rate: dimensionless air concentration and bubble count rate distributions: Smooth invert: $X=23.5$ m, $q_w=0.15$ m²/s; Stepped chute (Series 1): $X=21.2$ m (Step 9, $x=2$ m), $q_w=0.15$ m²/s; Stepped chute (Series 2): $X=20.4$ m (Step 16, $x=1.19$ m), $q_w=0.15$ m²/s.

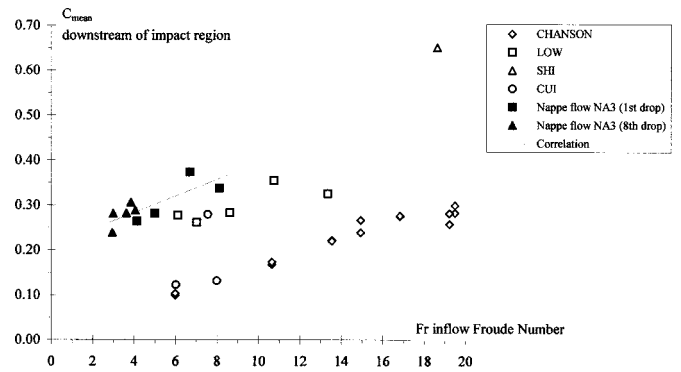


Fig. 10. Mean air concentration at the downstream end of the impact/spray region. Comparison between nappe flow NA3 data (1st and 8th drops) and spillway aeration device data (Table 3).

where F =inflow Froude number measured immediately upstream of the step brink (Fig. 10).

Summary and Conclusions

New experiments were conducted in a flat stepped chute that is very similar to stepped storm waterways, drains, and culverts. Physical modeling was based upon a Froude similitude and the large size of the facility ensures negligible scale effects. Three basic flow regimes were observed: nappe flow without hydraulic jump for $0.24 < d_c/h < 1$, transition flow for $d_c/h = 1.2$, and skimming flow for $dc/h \geq 1.5$.

In nappe flow, interfacial aeration occurs along the upper and lower nappe [Eqs. (1) and (2)]. Downstream of nappe impact, spray, and splashing was observed followed by a decelerated supercritical flow until the downstream end of the step. The flow pattern has some similarity with spillway aeration device flows, although comparatively greater downstream aeration was observed (Fig. 10). The transition flow did not have the quasismooth appearance of skimming flow nor the successive free-falling nappes of nappe flow. At each step brink, no air cavity was observed but very significant splashing was observed downstream of the stagnation point, giving a chaotic appearance to the flow. Although large air concentrations were measured, the bubble count rate data suggest relatively larger droplet and bubble sizes than in nappe and skimming flows. In skimming flow, the free-surface profile exhibited an undular profile in phase with the stepped

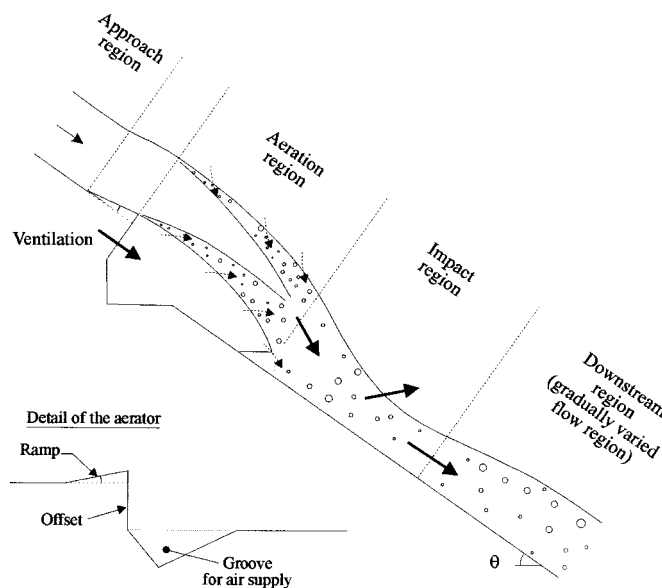


Fig. 9. Sketch of a spillway aeration device flow

Table 3. Spillway Aeration Device Configurations for Air Concentration Measurements

Reference	Slope θ (deg)	Offset height (m)	Ramp height (m)	Ramp angle (deg)	W (m)	d_o (m)	F_0
Shi et al. (1983)	49.0	0.0	0.015	5.7	0.20	0.06	14
Cui (1985)	0.0	0.0	0.015	5.7	0.20	0.12	8.9
	30.0	0.0	0.015	5.7	0.20	0.15	6.0
	49.0	0.0	0.015	5.7	0.20	0.12	7.5
Low (1986)	51.3	0.030	0.030	5.7	0.25	0.05	7 to 11
Chanson (1989a,b)	52.3	0.030	0.0	0.0	0.25	0.02	24
	52.3	0.030	0.0	0.0	0.25	0.03	13 to 21
	52.3	0.030	0.0	0.0	0.25	0.07	7.5

Notes: W =channel width and F_0 =inflow Froude number.

invert. The air concentration distributions had the same shape as in smooth-invert chute flows [Eq. (3)] although greater aeration was consistently observed in skimming flows.

The rate of energy dissipation was significant for all flow rate (i.e., $\Delta H/H \sim 0.8$, Table 2). Eq. (8) provides an estimate of the dimensionless residual head. For two chute slopes ($\theta = 3.4$ and 5.7°), the modified friction slope ($8^*S_f/F^2$) was about 2.5 times greater than the friction factor f of the smooth-chute flow.

A comparison between smooth and stepped-invert flows shows that greater aeration and larger residence times take place in the latter geometry. The result confirms the air–water mass transfer potential of stepped cascades, even for flat slope ($\theta < 5^\circ$).

Acknowledgments

The writers thank M. Condon, M. Eastman, L. Rowlands, and N. Van Schagen (University of Queensland) for their assistance and Dr. Y. Yasuda for providing his experimental data. They acknowledge the help of G. Illidge (University of Queensland) and the helpful discussion with Professor C. J. Apelt. One of the writers (H.C.) thanks Professor Colin O'Connor (University of Queensland) for alerting him of the Minoan bridge in Knossos.

Notation

The following symbols are used in this paper:

- C = air concentration, or void fraction;
- C_{mean} = mean air concentration: $(1 - C_{\text{mean}})Y_{90} = d$;
- D_t = air bubble turbulent diffusivity (m^2/s);
- D' = dimensionless turbulent diffusivity;
- d = clear-water flow depth: $d = \int_0^{Y_{90}} (1 - C) dy$;
- d_c = critical flow depth (m) assuming a hydrostatic pressure distribution and uniform velocity distribution; in rectangular channel: $d_c = \sqrt[3]{q_w^2/g}$;
- F = bubble count rate (Hz);
- F_{max} = maximum bubble count rate (Hz) in section;
- F = Froude number: $F = q_w \sqrt{gd^3}$;
- f = 1-Darcy–Weisbach friction factor;
- 2-modified friction slope: $f = 8^*S_f/F^2$;
- g = gravity acceleration (m/s^2) $g = 9.80 \text{ m}/\text{s}^2$ in Brisbane, Australia;
- H = total head (m);
- H_{res} = residual specific energy (m);
- h = step height (m);
- K' = dimensionless integration constant;
- k = dimensionless parameter;
- k_s = equivalent sand roughness height (m);
- L = chute length (m);
- l = step length (m);
- q_w = water discharge per unit width (m^2/s);
- S_f = friction slope;
- U_w = average flow velocity (m/s): $U_w = q_w/d$;
- V = velocity (m/s);
- V_c = critical flow velocity (m/s): $V_c = \sqrt{gd_c}$;
- W = chute width (m);
- X = longitudinal distance (m) measured from intake;
- x = longitudinal distance (m) measured from each step vertical face;

- Y_{50} = characteristic vertical distance where $C = 50\%$;
- Y_{90} = characteristic vertical distance where $C = 90\%$;
- y = vertical distance (m) measured from each step horizontal face;
- z_0 = invert elevation (m);
- ΔH = head loss (m);
- θ = channel slope;
- ρ_w = water density (kg/m^3);
- σ = surface tension between air and water (N/m); and
- τ_0 = boundary shear stress (Pa).

Subscript

- 0 = intake flow conditions.

References

- Brattberg, T., Chanson, H., and Toombes, L. (1998). "Experimental investigations of free-surface aeration in the developing flow of two-dimensional water jets." *J. Fluids Eng.*, 120(4), 738–744.
- Chanson, H. (1989a). "Study of air entrainment and aeration devices." *J. Hydraul. Res.*, 27(3), 301–319.
- Chanson, H. (1989b). "Flow downstream of an Aerator. Aerator spacing." *J. Hydraul. Res.*, 27(4), 519–536.
- Chanson, H. (1995a). *Hydraulic design of stepped cascades, channels, weirs, and spillways*, Pergamon, Oxford.
- Chanson, H. (1995b). "Air bubble entrainment in free-surface turbulent flows. Experimental investigations." *Rep. No. CH46/95*, Dept. of Civil Engineering, Univ. of Queensland, Australia.
- Chanson, H. (1996). "Prediction of the transition nappe/skimming flow on a stepped channel." *J. Hydraul. Res.*, 34(3), 421–429.
- Chanson, H. (1997a). *Air bubble entrainment in free-surface turbulent shear flows*, Academic, London.
- Chanson, H. (1997b). "Air bubble entrainment in open channels. Flow structure and bubble size distributions." *Int. J. Multiphase Flow*, 23(1), 193–203.
- Chanson, H., and Brattberg, T. (2000). "Experimental study of the air–water shear flow in a hydraulic jump." *Int. J. Multiphase Flow*, 26(4), 583–607.
- Chanson, H., and Toombes, L. (1997). "Energy dissipation in stepped waterway." *Proc., 27th IAHR Congress*, San Francisco, Vol. D, F. M. Holly Jr. and A. Alsaffar, eds., 595–600.
- Cui, L. (1985). "Air concentration distribution downstream of aeration ramp." *Shuili Xuebao (J. Hydraul. Eng.)*, Beijing, China, 1, 45–50 (in Chinese).
- Evans, A. H. (1928). *The Palace of Minos: A comparative account of the successive stages of the early Cretan civilization as illustrated by the discoveries at Knossos*, Vol. II, Part 1, Macmillan, London.
- Kazempour, A. K., and Apelt, C. J. (1983). "Effects of irregularity of form on energy losses in open channel flow." *Aust. Civil Eng. Trans.*, Vol. CE25, Institution of Engineers, Australia, 294–299.
- Low, H. S. (1986). "Model studies of clyde dam spillway aerators." *Research Rep. No. 86-6*, Dept. of Civil Engineering, Univ. of Canterbury, Christchurch, New Zealand.
- Noori, B. M. A. (1984). "Form drag resistance of two dimensional stepped steep open channels." *Proc., 1st Int. Conf. on Hydraulic Design in Water Resources Engineering*, Channels and Channel Control Structures, Southampton, U.K., K. V. H. Smith, ed., Springer, Berlin, 1.133–1.147.
- Ohtsu, I., and Yasuda, Y. (1997). "Characteristics of flow conditions on stepped channels." *Proc., 27th IAHR Biennial Congress*,

San Francisco, Theme D, 583–588.

Rajaratnam, N. (1990). “Skimming flow in stepped spillways.” *J. Hydraul. Eng.*, 116(4), 587–591.

Robison, R. (1994). “Chicago’s waterfalls.” *Civ. Eng.*, 64(7), 36–39.

Shi, Q., Pan, S., Shao, Y., and Yuan, X. (1983). “Experimental investigation of flow aeration to prevent cavitation erosion by a deflector.” *Shuili Xuebao (J. Hydraul. Eng.)*, Beijing, China, 3, 1–13

(in Chinese).

Wood I. R. (1991). “Air entrainment in free-surface flows.” *IAHR hydraulic structures design manual no. 4*, Hydraulic Design Considerations, Balkema, Rotterdam, The Netherlands.

Yasuda, Y., and Ohtsu, I. O. (1999). “Flow resistance of skimming flow in stepped channels.” *Proc., 28th IAHR Congress*, Graz, Austria, Session B14.